Bulletin of the Seismological Society of America, Vol. 105, No. 6, pp. 3189–3195, December 2015, doi: 10.1785/0120150149

Short Note

Long Valley Caldera and the UCERF Depiction of Sierra Nevada Range-Front Faults

by David P. Hill and Emily Montgomery-Brown

Abstract Long Valley caldera lies within a left-stepping offset in the north-northwest-striking Sierra Nevada range-front normal faults with the Hilton Creek fault to the south and Hartley Springs fault to the north. Both Uniform California Earthquake Rupture Forecast (UCERF) 2 and its update, UCERF3, depict slip on these major range-front normal faults as extending well into the caldera, with significant normal slip on overlapping, subparallel segments separated by ~10 km. This depiction is countered by (1) geologic evidence that normal faulting within the caldera consists of a series of graben structures associated with postcaldera magmatism (intrusion and tumescence) and not systematic down-to-the-east displacements consistent with distributed range-front faulting and (2) the lack of kinematic evidence for an evolving, postcaldera relay ramp structure between overlapping strands of the two range-front normal faults. The modifications to the UCERF depiction described here reduce the predicted shaking intensity within the caldera, and they are in accord with the tectonic influence that underlapped offset range-front faults have on seismicity patterns within the caldera associated with ongoing volcanic unrest.

Introduction

In a collaborative effort, the U.S. Geological Survey (USGS) and the California Geological Survey published an estimate of shaking hazards associated with scenario earthquakes in the Long Valley caldera (LVC)–Mono Lake area (Chen *et al.*, 2014). The scenario earthquakes are based on the Uniform California Earthquake Rupture Forecast 2 (UCERF2) fault model (Field *et al.*, 2009). LVC lies within a left-stepping offset in the north-northwest-striking range-front normal faults with the Hilton Creek fault (HCF) to the south and Hartley Springs fault (HSF) to the north. Both UCERF2 and its update, UCERF3 (Field *et al.*, 2015), depict slip on these major range-front normal faults as extending well into the caldera with significant normal slip on overlapping, subparallel segments separated by ~10 km (dotted lines in Fig. 1). This depiction is taken from the 2008 National Seismic Hazard Map (NSHM) (see Data and Resources). The time-independent UCERF3 was absorbed into the 2014 NSHM, and therefore future scenario earthquakes for the Long Valley region will come from UCERF3, which will likely include the type of events discussed in this article, as well as many more events involving these faults linking up with other faults ranked by their relative probabilities. Faults at the scale of this map are drawn through fault zones as a single trace, representing an average trend of multiple, subparallel mapped traces. The HSF and HCF within the topographic bounds of LVC are drawn to represent an average trend through zones of subparallel fault traces as compiled by Sawyer and Bryant (1995) and Sawyer (1995), respectively, in the USGS Quaternary Fault and Fold Database (QFFD). It is worth noting that in the QFFD, the HCF is represented as a red line that splays into the caldera; with red indicating movement in the last 150 years. This young date is apparently based on the distribution of surficial cracks in unconsolidated colluvium induced by shaking from the four **M** ~ 6 Mammoth Lakes earthquakes of May 1980 (Taylor and Bryant, 1980; Clark *et al.*, 1982; M. M. Clark, personal comm., 2015). The 1980 earthquakes were dominantly strike slip, and all were located in the Sierra Nevada west of the east-dipping HCF (Prejean *et al.*, 2002).

The UCERF depiction is countered by (1) geologic observations of faulting patterns and magmatism within the caldera and (2) the kinematics of a left-stepping offset between east-dipping normal faults with comparable slip rates. The modifications to the UCERF depiction proposed here reduce the predicted shaking intensity within the caldera, and they are in accord with the tectonic influence the offset range-front faults have on seismicity patterns within the caldera associated with ongoing volcanic unrest, as proposed by Prejean *et al.* (2002).

The LVC–Mono Craters (MC) volcanic field, located at the base of the eastern escarpment of the Sierra Nevada (Fig. 1), is the most productive source of late Cenozoic-to-recent volcanism in California and western Nevada (Bailey *et al.*, 1976; Hildreth, 2004; Hildreth *et al.*, 2014). This major volcanic field

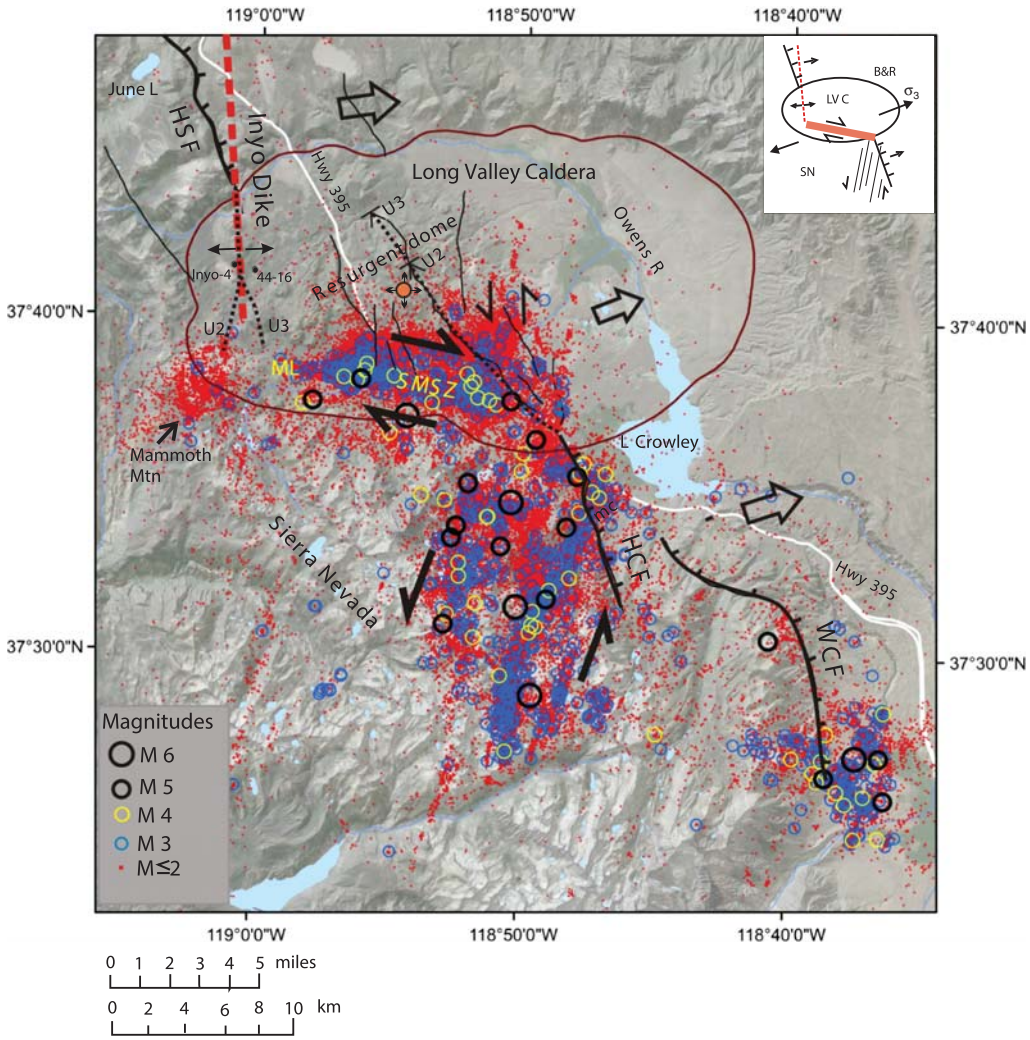

Figure 1. Shaded relief map of Long Valley caldera (LVC) area showing deformation sources and the kinematics of the offset between extensional zones across the caldera represented by the Hartley Springs fault (HSF)–Inyo dike to the north and the Hilton Creek fault (HCF) to the south, with the intervening South Moat seismic zone (SMSZ) as a leaky transform fault. Double-difference earthquake epicenters for $\mathbf{M} > 1$ seismicity from 1984–2014 scaled with size from dots ($\mathbf{M} \leq 2$) to large black circles ($\mathbf{M} \leq 5$). The solid orange circle with four opposing arrows is the location of the inflation source at 7 km depth beneath the resurgent dome. The heavy black lines are range-front normal faults, with barbs indicating slip direction: HSF, Hartley Springs fault; HCF, Hilton Creek fault; and WCF, Wheeler Crest fault. The dashed red line is the Inyo dike. Black dotted lines indicate the Uniform California Earthquake Rupture Forecast (UCERF) depictions of the HCF and HSF within Long Valley caldera (U2, UCERF2; U3, UCERF3). Drill holes Inyo-4 and Unocal 44-16 are indicated by small black circles on either side of the Inyo dike. Large open arrows indicate the approximate orientation of tectonic extension in the LVC region. ML indicates the town of Mammoth Lakes. (inset) Simplified diagram illustrating the dominant sources contributing to the local tectonic stress field in LVC and its vicinity. Long opposing arrows indicate the approximate orientation of the least principal tectonic stress σ_3, in the vicinity of LVC.

is situated at the west end of the Mina deflection, a right-stepping (releasing) offset linking the dextral eastern California shear zone with the Walker Lane dextral shear zone to the north (Hill, 2006; Riley *et al.*, 2012). LVC, the major source of volcanism within this field, is a 15 km × 30 km oval-shaped topographic depression formed 760 ka with the eruption of ~600 km^3 of rhyolitic Bishop tuff. Subsequent volcanic activity includes postcaldera extrusion of rhyolite domes forming the resurgent dome and moat rhyolites (700–100 ka), a sequence of dacitic and mafic eruptions forming Mammoth Mountain and associated mafic vents from 230 to 8 ka (Hildreth *et al.*, 2014), and a series of rhyolitic eruptions from ~65 ka to just ~250 yr B.P., forming the Mono–Inyo volcanic chain from Mono Lake into the west moat of the caldera (Bursik and Sieh, 1989; Bursik *et al.*, 2003; Vazquez and Lidzbarski, 2012).

Geologic Constraints

The Basin and Range extension north of the caldera is accommodated by a combination of normal slip on the HSF and dike intrusion beneath the subparallel Mono–Inyo volcanic chain. Mapped offsets on the HSF extend for 8 km southward from the vicinity of June Lake to the north margin

of the caldera (Bursik and Sieh, 1989; Bursik *et al.*, 2003). Normal slip on the fault has produced an ~100 m vertical offset of the 760 ka Bishop tuff (W. Hildreth, mapping in progress, 2015). The Mono–Inyo volcanic chain is ~50 km long, extending southward from Paoha Island in Mono Lake midway into the west moat of the caldera (Bursik and Sieh, 1989; Bursik *et al.*, 2003). Bursik and Sieh (1989) conclude that slip on the HSF diminished significantly at ~40 ka as the onset of dike intrusion beneath the Mono–Inyo chain began to accommodate much of the extension across this zone. Table 2 in Bursik *et al.* (2003) gives the Holocene vertical slip rate on the fault as ~0.1 mm/yr, which, for a fault dip of ~60°, corresponds to an extension rate of only ~0.06 mm/yr. Bursik *et al.* (2003) cite evidence that the 650 ka Mono–Inyo dome eruptions were accompanied by a series of strong (**M** ~ 5–6) earthquakes on the HSF in a volcanotectonic cascade as the stresses associated with the southward-propagating dike began interacting with the fault to trigger earthquakes, which in turn, triggered eruptions from the Inyo vents within the west moat of the caldera.

The UCERF depiction of the HSF extends well into the west moat of the caldera, coinciding closely with the trend of the Inyo volcanic vents (Fig. 1) and the series of short normal faults with opposing dips forming grabens associated with intrusion of the dike that fed the Inyo eruptions 600–625 yr B.P. (Bailey *et al.*, 1976; Bursik and Seih, 1989, 2013; Bursik *et al.*, 2003; Hildreth, 2004; Hildreth *et al.*, 2014). The UCERF2 depiction extends the HSF to Highway 203 near the base of Mammoth Mountain, whereas the UCERF3 depiction has it extending to within 1 km of Mammoth Lakes and the "Earthquake Fault," an extension fracture with no vertical offset. The Inyo-4 slant borehole (drilled just west of the South Inyo crater) and borehole Unocal 44-16 (located 0.9 km to the east-southeast) both intersect the ~700 ka early rhyolite at similar elevations consistent with no significant vertical offset across the intervening area spanning the Inyo volcanic chain (Eichelberger *et al.*, 1988) and the UCERF depictions of the HSF. The depth to crystalline basement rock (Mesozoic metavolcanics), however, is ~900 m deeper in Unocal 44-16 than in Inyo-4, which may represent (1) slip on the ring-fracture system formed during caldera collapse, (2) slip on a precaldera southern extension of the HSF, or (3) Inyo-4 intersecting a landslide block of basement rock deposited during or shortly after caldera collapse (Eichelberger *et al.*, 1988). Thus, although significant normal slip on the HSF apparently has not extended into the caldera since its formation 760 ka, the Inyo dike extends the colinear extension zone midway into the west moat of the caldera as a local spreading center.

The Holocene extension rate across intrusion of the Inyo dike remains uncertain. The Inyo-4 drill hole intersected a 7- to 8-m-wide breccia zone above the Inyo dike at a depth of ~600 m beneath the South Inyo crater (Eichelberger *et al.*, 1988). Mastin and Pollard (1988) estimate that the total extension across the intrusion zone to be ~20 m or more, based on structural analysis of the surface faults associated with the intrusion. An ~15 m extension across the Inyo intrusion zone within the caldera would match the ~0.6 mm/yr Holocene extension rate attributed to a section of the Sierra Nevada range-front fault system adjacent to the caldera (Rood *et al.*, 2011).

South of the caldera, normal slip on the HCF accommodates Basin and Range extension with respect to the Sierra Nevada. The HCF cuts the McGee Creek glacial moraine with ~15–17 m of down-to-the east-northeast postglacial dip-slip 5 km south of the caldera boundary corresponding to a vertical slip rate of 0.9–1.2 mm/yr over the past 14 ka (Berry, 1997). This corresponds to an extension rate of ~0.6 mm/yr for a fault dip of ~60°. The UCERF-depicted extension of the HCF into the caldera cuts across the ~700 ka rhyolite flows forming the resurgent dome, which show no evidence of significant down-to-the east normal faulting. Indeed much of the depicted UCERF trace coincides with a west-dipping normal fault associated with a medial graben formed in response to uplift of the resurgent dome (Bailey *et al.*, 1976).

In short, geologic evidence for the relation between patterns of postcaldera normal faulting and magmatism within the caldera does not support significant postcaldera (< 760 ka) range-front slip on either the HSF or HCF as extending into the caldera.

Kinematic Constraints

The deformation style in the offset between left-stepping normal faults depends on the extent of the strike-parallel overlap between the faults. The idealized geometry illustrated in Figure 2 is for faults with comparable dips and slip rates or, in the case of Figure 2a (right), a dike and a normal fault with comparable extension rates:

1. Deformation along an oblique link between underlapping fault tips (Fig. 2a, left) or a dike and a fault (Fig. 2a, right) is transtensional, involving strike-slip displacement with an extensional component, which could be accompanied by either opening and intrusion (as in a leaky transform fault) or a dip-slip component on a normal fault dipping to the north-northeast.
2. Deformation along an orthogonal link between adjacent fault tips involves dextral strike slip on a vertical fault with a component of normal slip accommodating the dip-slip displacement of the normal-fault hanging wall.
3. Deformation between overlapping fault tips is accommodated by a relay ramp (gray trapezoid), the detailed morphology of which depends on the strike, rake, and displacement gradients toward the tips of the overlapping faults (Ferrill and Morris, 2001). For a left-stepping offset between east-dipping faults, a ramp undergoes clockwise rotational strain and may be ruptured by one or more breaching faults in the area of steepest dip (darker gray shading).

An oblique, left-stepping offset linking the HCF and southern end of the Inyo dike (Fig. 2a, right) is consistent with seismicity and deformation patterns associated with caldera unrest

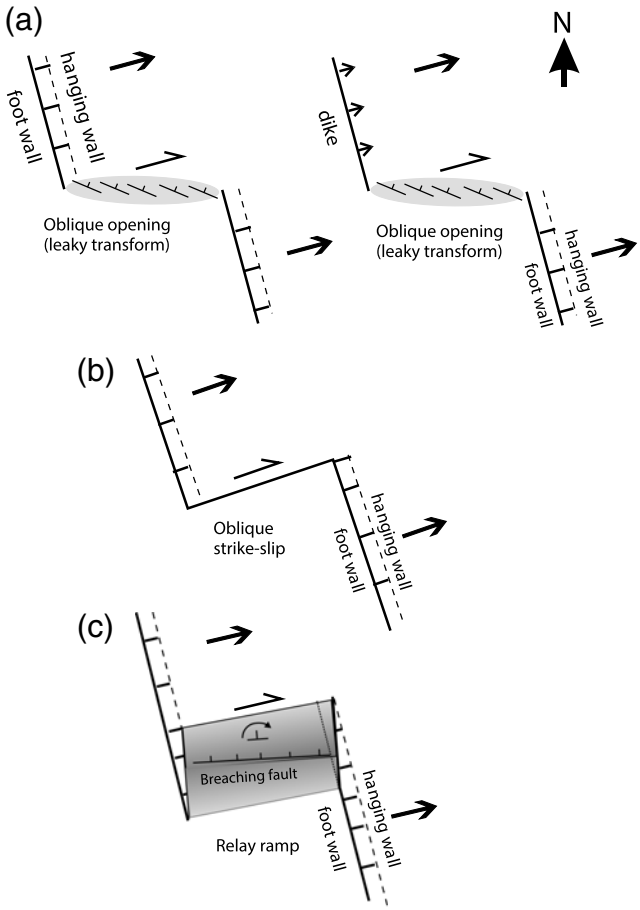

Figure 2. Idealized map-view schematic illustrating the kinematics of left-stepping offsets between normal fault segments with the same dip and slip rate. Barbs indicate the relative displacement of the hanging-wall block with respect to the footwall block. The footwall block (Sierra Nevada) is regarded as fixed with respect to the northeast displacement of the hanging-wall block (Basin and Range). Arrows indicate the direction of slip or displacement. (a) Underlapped offset forms an obtuse angle between adjacent fault tips, resulting in oblique opening accommodated by en echelon dextral strike-slip fault dipping to the northeast (a leaky transform fault indicated by the gray zone): (left) underlap offset between normal faults, and (right) underlap offset between a dike intrusion and a normal fault. Small arrows indicate the opening direction of dike. (b) Orthogonal offset forms a right angle between adjacent fault segments, resulting in oblique dextral slip on a transform fault with an oblique rake that is either vertical or dipping to the northwest. (c) An overlapped offset forms an acute angle between the tips of adjacent normal fault segments. Deformation between overlapping fault segments develops as a relay ramp (shaded trapezoid) dipping to the north, the length of which is governed by the horizontal gradient in slip rates toward opposing normal-fault tips. Dip steepness along the ramp is indicated by darker shading. Breaching faults may form in the zone of steepest dips.

(Prejean *et al.*, 2002). Neither the modern topography nor late Cenozoic faulting patterns reflect the kinematics of a relay ramp (Fig. 2c) between overlapping range-front faults within the caldera, as depicted by the UCERF representations.

Seismic refraction and gravity surveys, however, support the Bailey (1989) inference that a relay ramp likely existed between the en echelon HSF and HCF prior to the 760 ka caldera-forming eruption. Data from both sets of geophysical surveys indicate down-to-the east displacement of the crystalline basement along a northward extension of the HCF beneath the east moat of the caldera and a downward tilt to the north of the basement beneath the north-central part of the caldera (Hill, 1976; Abers, 1985; Hill *et al.*, 1985; Carle, 1988). As Bailey (1989) suggested, caldera collapse along the ring-fracture system and underlying residual magma body apparently modified the interaction of the regional stresses with the down-dropped cauldron block and its tectonic-magmatic evolution following the 760 ka Bishop tuff eruption. Crustal extension accompanying intrusions feeding the eruptions of Mammoth Mountain, its associated field of mafic vents, and the Inyo volcanic chain from ~230 ka to ~600 yr B.P. apparently muted range-front normal faulting along the western margin of the caldera.

Range-Front Faults and Caldera Unrest

The onset of caldera unrest in May 1980 included strong earthquake swarm activity in the southern section of the caldera and the Sierra Nevada block to the south, together with inflation of the resurgent dome in the center of the caldera by 25 cm (Hill, 2006). This basic unrest pattern has persisted to date with varying intensity with the cumulative uplift of the resurgent dome currently exceeding 80 cm. Deformation associated with resurgent dome inflation is radially symmetric about the center of the resurgent dome, with a diameter of ~10 km. Langbein (2003) and Montgomery-Brown *et al.* (2015) model resurgent dome inflation as driven by a volume increase of a prolate spheroid centered at a depth of ~7 km beneath the resurgent dome (Figs. 1, and 3), with a possible secondary contribution from a deeper source (12 km) beneath the South Moat seismic zone (SMSZ) (not shown in Fig. 1). Earthquake swarm activity within the caldera, however, is largely confined to a west-northwest-striking zone in the south moat (the SMSZ in Fig. 1).

High-resolution analysis of caldera seismicity reveals that swarm earthquakes in the SMSZ are aligned in subparallel, west-northwest-striking lineations (Prejean *et al.*, 2002; Lin, 2015). The swarm earthquakes show dominantly dextral strike-slip focal mechanisms with *T* axes oriented to the north-northeast and with some mechanisms showing a volumetric component consistent with aqueous fluid transport (Dreager *et al.*, 2000; Prejean *et al.*, 2002). Prejean *et al.* (2002) conclude that the earthquakes occur in response to a regional tectonic stress field rather than the local stress field produced by inflation of the resurgent dome. They suggested that the kinematics of an oblique offset between the southern end of the Inyo dike and the northern end of the HCF, linked by a leaky transform fault through the south moat (compare our Fig. 2a, left, and fig. 14 in Prejean *et al.*, 2002), is a likely source for this tectonic stress field. Notably, the Langbein (2003) inversion of trilateration and Global Positioning System (GPS) deformation data within the caldera for 1988–2001

shows over 2 m of dextral offset across the SMFZ, much of which accumulated during the 1997–1998 south-moat earthquake swarm activity (fig. 10 in Langbein, 2003).

Although regional tectonic stresses appear to control the orientation and sense of slip for earthquakes within the SMSZ, the level of earthquake swarm activity generally varies with the inflation rate of the resurgent dome. The onset of increased swarm activity generally lags behind the onset of an inflation episode by days to weeks (Hill *et al.*, 2003). A plausible explanation is that south-moat swarm activity is modulated by episodes of resurgent dome inflation through the release of hydrous magmatic fluids from the pressure source at depth. The elevated pore pressure of the hydrous fluids propagates upward as a diffusive front, triggering brittle failure within the fracture mesh forming the dextral leaky transform fault zone through the south moat.

Riley *et al.* (2012) propose a similar geometry for a leaky transform fault through the south moat. They, however, appeal to a left-stepping offset in a spreading center across the caldera between the Inyo dike to the north and a hypothetical spreading center extending southward into the footwall of the HCF in the Sierra Nevada. The seismicity in the Sierra Nevada south of the caldera, however, consists of north-northeast-trending lineations defining near-vertical, sinistral faults in the footwall of the HCF (Prejean *et al.*, 2002). The evidence for a spreading center there is based on the controversial non-double-couple focal mechanisms for two of the three May 1980 **M** 6 earthquakes in the Sierra Nevada south of the caldera (Julian and Sipkin, 1985; Wallace, 1985). If such a structure exists, it has yet to produce surface expression. Normal slip on the HCF dominates late Cenozoic extension across the Sierra Nevada–Basin and Range boundary south of the caldera.

Comparing Tectonic and Magmatic Stresses

An estimate of the fault-parallel shear stress acting on the west-northwest-striking SMFZ imposed by inflation of the resurgent dome can provide a constraint on magnitude of the tectonic stress driving dextral slip within the fault zone. The preferred model for the volumetric source driving inflation of the resurgent dome is a vertical, prolate spheroid centered at a depth of ~7 km, based on inversion of GPS and InSAR data from 2011 to 2014 (Montgomery-Brown *et al.*, 2015). Because the current inflation source is essentially indistinguishable from those inferred using earlier geodetic data, we fix the source geometry and solve for stresses associated with the accumulated volume change in this source since the beginning of the geodetic observations in 1975 (Langbein, 1989, 2003). We model the source as a vertical prolate ellipsoid (3 km vertical radius and 1.5 km horizontal radii) under the resurgent dome in an elastic homogenous half-space with Poisson's ratio of 0.25 and shear modulus of 3×10^{10} N/m^2. The total accumulated extension of a line spanning the resurgent dome between GPS sites CA99 and KRAC (Fig. 3) is 0.86 m, which closely matches the cumulative uplift of the central section of the resurgent dome determined by repeat leveling surveys. This deformation is consistent with a cumulative increase in the source volume of 3.4×10^8 m^3 since 1980.

The resulting shear stress τ, resolved on vertical, west-northwest-striking planes at a depth of 7 km is a four-lobed pattern with right-lateral slip encouraged on faults in the eastern section of the SMSZ and opposed in the western section (Fig. 3). The magnitude of τ, opposing dextral slip on faults in the western sector of the SMSZ, is ~3–4 MPa, assuming minimal stress relaxation over the 40 yr period. This implies a minimum bound on the tectonic stress driving dextral slip of ~5 MPa.

Implications for Earthquake and Volcanic Hazards

Chen *et al.* (2014) estimate shaking hazards for three scenario earthquakes on the HCF: (1) an **M** 6.9 scenario based on the UCERF2 model with rupture extending ~12 km into the caldera, (2) an **M** 6.6 with fault rupture extending 7 km into the caldera (alternative 1), and (3) an **M** 6.5 with rupture stopping at the caldera boundary (alternative 2). Only the last is consistent with the geologic constraints described above (see Fig. 1). The shaking intensity predicted by the alternative 2 scenario earthquake reduces the maximum modified Mercalli intensity (MMI) of 8.2–8.7 to MMI 7.7–8.2 in the area between the UCERF2 depiction of the fault and the Owens River.

The section in Chen *et al.* (2014) on the HSF is based solely on the UCERF-2 model, which terminates near the base of Mammoth Mountain 4 km west of Mammoth Lakes (dotted line labeled U2 in Fig. 1). The scenario **M** 6.7 earthquake for this version of the fault predicts an MMI of 8.2–8.5 in Mammoth Lakes and a spectral acceleration at 1.0 s of 50%–66%g. Using an alternative scenario earthquake with reduced fault length (from ~12 to ~8 km), together with termination of fault rupture at the caldera boundary ~8 km north of Mammoth Lakes as proposed here, would significantly reduced the predicted shaking intensity in the vicinity of the town from a scenario earthquake with respect to that of the UCERF2 model. A cautionary note, however; as noted by Bursik *et al.* (2003), rupture of the southern section of the HSF with one or more **M** ~ 5–6 earthquakes 650 yr B.P. apparently activated renewed intrusion along the Inyo dike in a volcanotectonic cascade, resulting in eruptions from vents along the Inyo volcanic chain within the west moat of the caldera.

Conclusions

The UCERF depiction of slip on the Hartley Springs and HCFs as extending into LVC is countered by (1) geologic evidence that normal faulting within the caldera consists of a series of graben structures associated with postcaldera magmatism (intrusion and tumescence) and not systematic down-to-the-east displacements consistent with distributed range-front faulting and (2) the lack of kinematic evidence for an evolving, postcaldera relay ramp structure between overlap-

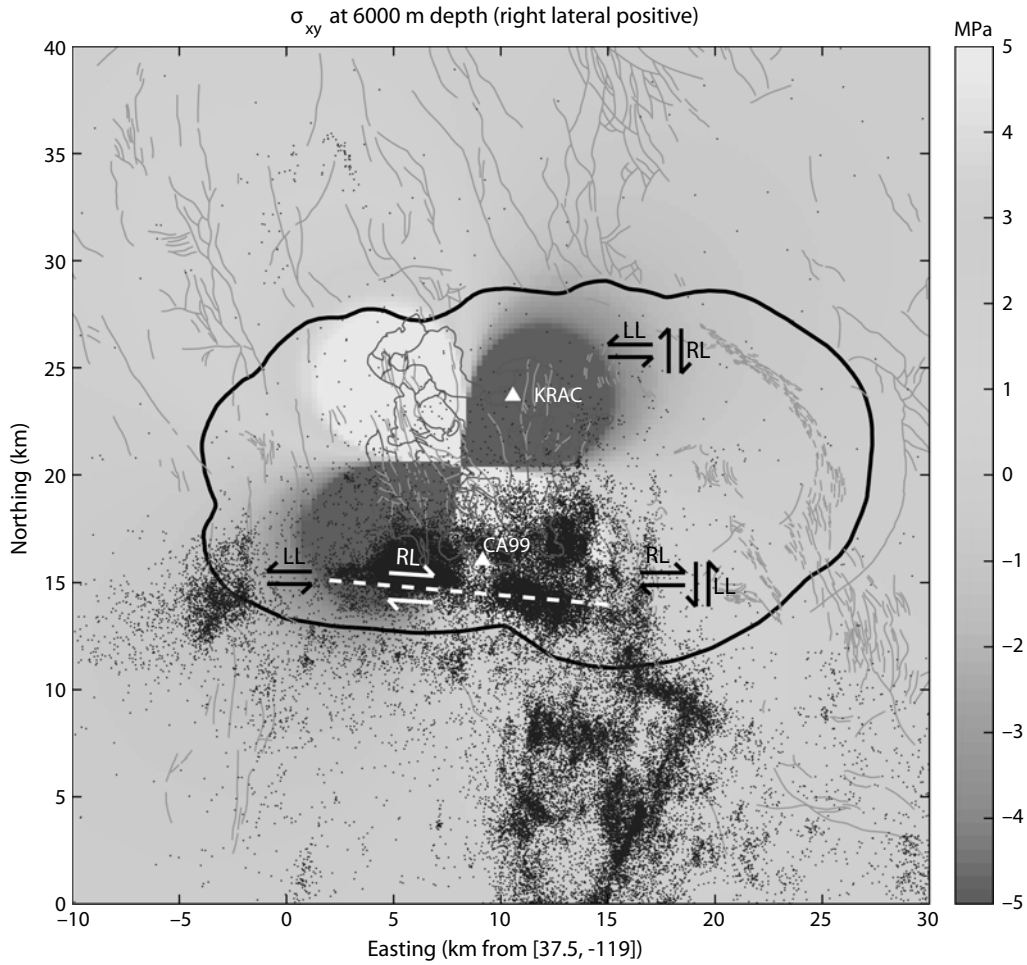

Figure 3. Estimated cumulative shear-stress change acting on west-northwest-striking faults (and their north-northeast-striking conjugates) at a depth of 7 km from 1975 to 2015, inferred from the cumulative inflation of the resurgent dome. Dark versus light shades indicate areas with enhanced dextral versus sinistral slip, respectively, as indicated by the black arrow couples. The white arrow couple indicates dextral slip across the South Moat fault zone (dashed line). The white triangles indicate Global Positioning System (GPS) sites CA99 and KRAC, which are collocated with former electronic distance-measurement (EDM) sites CASA and KRAK, respectively (see Langbein, 2003). Black dots are double-difference hypocentral locations for $\mathbf{M} > 2$ earthquakes spanning the same time period from the Northern California Earthquake Data Center (NCEDC) catalog (see Data and Resources).

ping strands of the two range-front normal faults (Fig. 2c). For the geometry initially proposed by Prejean *et al.* (2002) and illustrated in Figures 1 and 2a (right), the SMSZ is a leaky transform fault with dextral displacement forming an oblique link between the south end of the extension axis formed by a combination of normal slip on the HSF and MC dike intrusion north of the caldera boundary, dike intrusion within the west moat of the caldera, and normal slip on the HCF south of the caldera. Earthquake swarm activity within the leaky transform zone is driven by tectonic stresses associated with the offset between extension axes across the caldera. In turn, the seismicity rate within the SMSZ is modulated by surges in pore pressure driven by magmatic fluids expelled during inflation episodes of the resurgent dome.

The termination of postcaldera slip on the HSF and HCF at the caldera boundary results in shorter fault lengths, correspondingly smaller magnitudes, and lower shaking intensities in the vicinity of the caldera and the town of Mammoth Lakes with respect to those based on scenario earthquakes developed using the UCERF2 and UCERF3 fault representations.

Data and Resources

Computations were done using MATLAB (www.mathworks.com/products/matlab, last accessed October 2015). The U.S. Geological Survey (USGS) Quaternary Fault and Fold Database can be found at http://earthquake.usgs.gov/hazards/qfaults/map/hazfault2008.html (last accessed August 2015). The digital database of the Holocene tephras of the Mono–Inyo Craters, California, can be found at http://pubs.usgs.gov/ds/758/ (last accessed August 2015). Waveform data, metadata, or data products for this study were accessed through the Northern California Earthquake Data Center (NCEDC) (http://www.ncedc.org/ncedc/catalog-search.html, last accessed October 2015).

Acknowledgments

We are grateful for comments by Bill Ellsworth, Shaul Hurwitz, and Wes Hildreth on various drafts of the manuscript and for constructive reviews by Tim Dawson and an anonymous reviewer.

References

Abers, G. (1985). The subsurface structure of the Long Valley caldera, Mono County, California: A preliminary synthesis of gravity, seismic, and drilling information, *J. Geophys. Res.* **90,** 3627–3636.

Bailey, R. (1989). Geologic map of Long Valley Caldera, Mono-Inyo Craters volcanic chain, and vicinity, eastern California, *U.S. Geol. Surv. Map I-1933*, scale 1:62,500, 11 pp.

Bailey, R., G. B. Dalrymple, and M. A. Lanphere (1976). Volcanism, structure and geochronology of Long Valley Caldera, Mono County, California, *J. Geophys. Res.* **81,** 725–744.

Berry, M. E. (1997). Geomorphic analysis of late Quaternary faulting on Hilton Creek, Round Valley and Coyote warp faults, east-central Sierra Nevada, California, USA, *Geomorphology* **20,** 177–195.

Bursik, M., and K. Sieh (1989). Range front faulting and volcanism in the Mono basin, eastern California, *J. Geophys. Res.* **941,** no. B11, 15,587–15,609.

Bursik, M., and K. Sieh (2013). Digital database of the Holocene tephras of the Mono-Inyo Craters, California, *U.S. Geol. Surv. Data Series 758*.

Bursik, M., C. Renshaw, J. McCalpin, and M. Berry (2003). A volcanotectonic cascade: Activation of range front faulting and eruptions by dike intrusion, Mono basin-Long Valley Caldera, California, *J. Geophys. Res.* **108,** doi: 10.1029/2002JB002032.

Carle, S.F. (1988). Three-dimensional gravity modeling of the geologic structure of Long Valley Caldera, *J. Geophys. Res.* **93,** no. B11, 13,237–13,250.

Chen, R., D. M. Branum, C. J. Wills, and D. P. Hill (2014). Scenario earthquake hazards for the Long Valley Caldera—Mono Lake area, *Calif. Geol. Surv. Special Rept. 233, U.S. Geol. Surv. Open-File Rept. 2014-1045*, 92 pp., http://pubs.usgs.gov/of/2014/1045/pdf/ofr2014-1045.pdf (last accessed October 2015).

Clark, M. M., P. R. Vaughn, J. C. Yount, D. B. Burke, E. J. King, and J. C. Tinsley (1982). Surface ruptures, Mammoth Lakes, *Calif. U.S. Geol. Surv. Map MF-1396*, scale 1:24,000.

Dreager, D. S., H. Tkalcic, and M. Johnson (2000). Dilatational processes accompanying earthquakes in Long Valley caldera, *Science* **288,** 122–125.

Eichelberger, J. C., T. A. Vogel, L. W. Younger, C. D. Miller, G. H. Heiken, and K. H. Wholetz (1988). Structure and stratigraphy beneath a young phreatic vent: South Inyo Crater, Long Valley Caldera, California, *J. Geophys. Res.* **93,** 13,208–13,220.

Ferrill, D. A., and A. P. Morris (2001). Displacement gradient and deformation in normal fault systems, *J. Struct. Geol.* **23,** no. 4, 619–638.

Field, E. H., G. P. Biasi, P. Bird, T. E. Dawson, K. R. Felzer, D. D. Jackson, K. M. Johnson, T. H. Jordan, C. Madden, A. J. Michael, *et al.* (2015). Long-term time-dependent probabilities for the Third Uniform California Earthquake Rupture Forecast (UCERF3), *Bull. Seismol. Soc. Am.* **105,** 511–543, doi: 10.1785/0120140093.

Field, E. H., T. E. Dawson, K. R. Felzer, A. D. Frankel, V. Gupta, T. H. Jordan, T. Parsons, M. D. Petersen, R. S. Stein, R. J. Weldon, and C. J. Wills (2009). Uniform California Rupture Forecast, Version 2 (UCERF 2), *Bull. Seismol. Soc. Am.* 99**,** 2053–2107, http://pubs.usgs.gov/of/2007/1437/ (last accessed October 2015).

Hildreth, W. (2004). Volcanological perspectives on Long Valley, Mammoth Mountain, and Mono Craters: Several contiguous but discrete systems, *J. Volcanol. Geochem. Res.* **136,** nos. 3/4, 169–198.

Hildreth, W., J. Fierstein, D. Champion, and A. Calvert (2014). Mammoth Mountain and its mafic periphery—A late Quaternary volcanic field in eastern California, *Geosphere* **10,** 1315–1365, doi: 10.1130/GES01053.1.

Hill, D. P. (1976). Structure of Long Valley Caldera, California, from a seismic refraction experiment, *J. Geophys. Res.* **81,** 745–753.

Hill, D. P. (2006). Unrest in Long Valley Caldera, 1978-2004, in *Mechanisms of Activity and Unrest at Large Calderas*, C. Troise, G. DeNatale, and C. R. J. Kilburn (Editors), Geological Society Special Paper 269, London, United Kingdom, 1–24.

Hill, D. P., E. Kissling, J. H. Luetgert, and U. Kradolfer (1985). Constraints on the upper crustal structure of the Long Valley–Mono Craters volcanic complex, eastern California, from seismic refraction measurements, *J. Geophys. Res.* **90,** 11,135–11,150.

Hill, D. P., J. O. Langbein, and S. Prejean (2003). Relations between seismicity and deformation during unrest in Long Valley Caldera, California, from 1995 through 1999, *J. Volcanol. Geotherm. Res.* **127,** nos. 3/4, 175–193.

Julian, B. R., and S. A. Sipkin (1985). Earthquake processes in the Long Valley area, California, *J. Geophys. Res.* **90,** no. B13, 11,155–11,169.

Langbein, J. (1989). Deformation of the Long Valley Caldera, eastern California, from mid-1983 to mid-1988: Measurements using a two-color geodimeter, *J. Geophys. Res.* **94,** no. B4, 3833–3849.

Langbein, J. (2003). Deformation of Long Valley Caldera, California: Inferences from measurements from 1988 to 2001, *J. Volcanol. Geotherm. Res.* **127,** nos. 3/4, 247–267.

Lin, G. (2015). Seismic velocity structure and earthquake relocation for the magmatic system beneath Long Valley Caldera, eastern California, *J. Volcanol. Geotherm. Res.* **296,** 19–30.

Mastin, L. G., and D. D. Pollard (1988). Surface deformation and shallow dike intrusion processes at Inyo Craters, Long Valley, California, *J. Geophys. Res.* **93,** no. B11, 13,221–13,235.

Montgomery-Brown, E. K., C. W. Wicks, P. F. Cervelli, J. O. Langbein, J. L. Svarc, D. R. Shelly, D. P. Hill, and M. Lisowski (2015). Renewed inflation of Long Valley Caldera, California: 2011–2014, *Geophys. Res. Lett.* **42,** no. 13, 5250–5257, doi: 10.1002/2015GL064338.

Prejean, S., W. L. Ellsworth, M. Zoback, and F. Waldhouser (2002). Fault structure and kinematics of the Long Valley Caldera region, CA, revealed by high-accuracy earthquake hypocenters and focal mechanism stress inversions, *J. Geophys. Res.* **107,** no. B12, doi: 10.1029/2001JB001168.

Riley, P., B. Tikoff, and W. Hildreth (2012). Transtensional deformation and structural control of contiguous but independent magmatic systems: Mono-Inyo Craters, Mammoth Mountain, and Long Valley Caldera, California, *Geosphere* **8,** 740–751, doi: 10.1130/GES00662.1.

Rood, D. H., D. W. Burbank, and R. C. Finkel (2011). Spatiotemporal patterns of fault slip rates across the central Sierra Nevada frontal fault zone, *Earth Planet. Sci. Lett.* **301,** nos. 3/4, 457–468.

Sawyer, T. L. (Compiler) (1995). Fault number 44, Hilton Creek fault, in Quaternary Fault and Fold Database of the United States, *U.S. Geol. Surv.*, http://earthquakes.usgs.gov/hazards/qfaults (last accessed August 2015).

Sawyer, T. L., and W. A. Bryant (Compilers) (1995). Fault number 43, Hartley Springs fault zone, in Quaternary Fault and Fold Database of the United States, *U.S. Geol. Surv.*, http://earthquakes.usgs.gov/hazards/qfaults (last accessed 10 August 2015).

Taylor, G. C., and W. A. Bryant (1980). Surface rupture associated with Mammoth Lakes earthquakes of 25 and 27 May 1980, in *Mammoth Lakes Earthquakes of May 1980*, R. W. Sherburne (Editor), *Calif. Div. Mines Geol. Sp. Rept. 150*, 49–67.

Vazquez, J. A., and M. L. Lidzbarski (2012). High-resolution tephrochronology of the Wilson Creek Formation (Mono Lake, California) and Laschamp event using 238U-230Th SIMS dating of accessory mineral rims, *Earth Planet. Sci. Lett.* **357/358,** 54–67.

Wallace, T. C. (1985). A reexamination of the moment tensor solutions of the 1980 Mammoth Lakes earthquakes, *J. Geophys. Res.* **90,** 11,171–11,176.

U.S. Geological Survey
Volcano Science Center
MS 910 Menlo Park, California 943025
hill@usgs.gov
emontgomery-brown@usgs.gov

Manuscript received 28 September 2015;
Published Online 10 November 2015